N87-23330

ELECTRIC POTENTIAL DISTRIBUTIONS AT THE INTERFACE BETWEEN PLASMASHEET CLOUDS

D. S. Evans
NOAA/SEL
325 Broadway
Boulder, Colorado 80303, U.S.A.

and

M. Roth and J. Lemaire
Institut d'Aéronomie Spatiale de Belgique
3 av. Circulaire
B-1180 Bruxelles, Belgium

ABSTRACT

At the interface between two plasma clouds with different densities, temperatures, and/or bulk velocities, there are large charge separation electric fields which can be modeled in the framework of a collisionless theory for tangential discontinuities (see Lemaire and Burlaga, 1976; Roth, 1980; Botticher et al., 1983).

Two different classes of layers have been identified: the first one corresponds to (stable) ion layers which are thicker than one ion Larmor radius; the second one corresponds to (unstable) electron layers which are only a few electron Larmor radii thick.

We suggest that these thin electron layers with large electric potential gradients (up to 400 mV/m) are the regions where large-amplitude electrostatic waves are spontaneously generated. These waves scatter the pitch angles of the ambient plasmasheet electron into the atmospheric loss cone. The unstable electrons layers can therefore be considered as the seat of strong pitch angle scattering for the primary auroral electrons.

I. INTRODUCTION

Lyons and Evans (1984) found direct evidence from coordinated auroral and magnetospheric particle observations that discrete auroral arcs are located along geomagnetic field lines mapping in plasmasheet regions where significant spatial gradients in the magnetospheric particles velocity distribution are observed.

These observations as well as earlier theoretical calculations by Lemaire and Burlaga (1976) and Roth (1976, 1978, 1979, 1980) have motivated the present application of kinetic plasma theory to thin layers separating a hot plasmasheet cloud from a cooler background or another cloud which is populated with ions and electrons of different densities and temperatures. However, we do not simulate the magnetic field reversal region in the neutral sheet of the magnetotail.

We briefly recall the basic features of the kinetic model as well as the boundary conditions in the next section. The numerical results are presented in Section III; the discussion of this solution is given in the last section with the conclusions.

PRECEDING PAGE BLANK NOT FILMED

II. FORMULATION OF THE MODEL AND BOUNDARY CONDITIONS

The kinetic model used below is an extension of that proposed by Sestero (1964) to describe collisionless plasma sheaths in the laboratory. Although the plasmasheet is rarely in a stationary state, we assume that its structure does not change significantly over the characteristic period of time required for an Alfvén wave to traverse the transition layer.

Furthermore, it is assumed that the radius of curvature of the plasma sheath is much larger than its characteristic thickness, which is of the order of a few ion gyroradii. Under these circumstances the plasma layer can be considered as planar. Every physical quantity depends then on one space coordinate only, say x.

Since in general the magnetic field direction at the interface between plasmasheet diamagnetic irregularities does not vary by more than 10° or 20°, we consider that the direction of **B**, does not change nor reverse across the transition layer, but that **B** remains always parallel to the z-axis. The partial electric current densities ($j^{+,-}$) of the ions (+) and electrons (-) are then necessarily parallel to the y-axis. The electric field (as spatial gradient of the potential ϕ) is in the x-direction. Indeed we assume that, in a frame of reference fixed with respect to the plasma layer, there is no mass flow across nor toward the surface of discontinuity ($v_x = 0$).

In our kinetic model the ions and electrons from the left-hand side (i.e., side 1) have velocity distributions ($f_1^{+,-}$) which tend to an isotropic Maxwellian at $x = -\infty$. The zero-order moment (i.e., the density: $n_1^{+,-}$) of these distribution functions tends to an asymptotic density $N_1 = N_1^- = 0.5\ cm^{-3}$, at $x = -\infty$. The temperature of the ions and electrons $\theta_1^{+,-}$ from side 1 is determined by the second-order moments of $f_1^{+,-}$. When x tends to $-\infty$, $\theta_1^+(x)$ tends to $T_1^+ = 12$ keV, and $\theta_1^-(x)$ tends to $T_1^- = 2.5$ keV.

When x varies from $-\infty$ to $+\infty$ we expect $n_1^{+,-}$ to decrease to zero, and the velocity distributions $f_1^{+,-}$ to become depleted in the domain of the velocity space which is not accessible to the particles from side 1, i.e., for those particles with the smallest velocities and therefore the smallest gyroradii.

In absence of Coulomb collisions and wave-particle interactions, these velocity distributions are solutions to the collisionless Boltzmann-Vlasov equation. Any function of the constants of motion is then a solution. Following Sestero (1964) we choose for $f_1^{+,-}$ truncated distributions which tend to isotropic Maxwellians at $x = -\infty$, where $n_1^{+,-}$ and $\theta_1^{+,-}$ tend to the above given values for the densities and temperatures ($N_1^{+,-}$ and $T_1^{+,-}$), respectively.

When x tends to $+\infty$ the domains of the velocity space where $f_1^{+,-}$ differs from zero become vanishingly small; $n_1^{+,-}$ decreases then asymptotically to zero, as expected, because a smaller and smaller fraction of ions and electrons from side 1 has large enough gyroradius to penetrate deep into region 2 on the opposite side of the transition layer. For details see Roth et al. (1986).

Region 2 is populated with electrons and ions of a different origin, i.e., with different temperature distributions $\theta_2^{+,-}(x)$ and different density distributions $n_2^{+,-}(x)$. In our numerical calculation we have taken the following boundary conditions: $\theta_2^{+,-}(\infty) = T_2^{+,-}$ with $T_2^+ = 3$ keV and $T_2^- = 0.8$ keV; $n_2^{+,-}(\infty) = N_2^{+,-} = 0,15\ cm^{-3}$ and $n_2^{+,-}(-\infty) = 0$.

The velocity distributions $f_2^{+,-}$ of the ions and electrons originating from region 2 can again be any function of the constants of motion. As above, truncated Maxwellian velocity distributions are adopted. They tend to isotropic Maxwellians at $x = +\infty$, with densities and temperatures, respectively, equal to $N_2^{+,-}$ and $T_2^{+,-}$. When x tends to $-\infty$, $f_2^{+,-} \neq 0$ only for a decreasing number of particles from side 2 which has large enough velocities (and gyroradii) to penetrate deep inside region 1.

Note that the asymptotic behavior of the plasma distribution depends only on the asymptotic form of $f_{1,2}^{+,-}$ when x goes to $\pm\infty$. The form of $f_{1,2}^{+,-}$ for any other x in between is responsible for the shape of the transition profiles. Thus, the state of the plasma at one end of the transition region (or at both ends in our case) does not uniquely determine the plasma and field variation within the transition. This results from the collisionless and adiabatic nature of the interaction between the plasma particles. In a collision-dominated plasma when irreversible processes are important, this would not, however, be the case; the transition profile is then uniquely determined by the boundary conditions.

The moments of $f_{1,2}^{+,-}$ are integrals over the domain of velocity space where $f_{1,2}^{+,-}$ is not equal to zero. The densities $n_{1,2}^{+,-}(x)$ are the zero-order moments of $f_{1,2}^{+,-}$; the partial current densities ($j_{1,2}^{+,-} = eZ^{+,-} n_{1,2}^{+,-} \cdot v_{1,2}^{+,-}$) are first-order moments, etc. These moments are analytical expressions depending on x through the electric potential $\phi(x)$ and the magnetic vector potential a(x). Indeed, both $\phi(x)$ and a(x) appear explicitly in the constants of motion and consequently in $f_{1,2}^{+,-}$. The analytic expressions for $n_{1,2}^{+,-}$ and $j_{1,2}^{+,-}$ are similar to those derived by Sestero (1964, 1966). They are given in the more detailed article by Roth et al. (1986).

The electric potential $\phi(x)$ must satisfy Poisson's equation. However, in non-relativistic plasmas, where the thermal velocity of the ions and electrons is much smaller than the speed of light, Sestero (1966) has shown that a satisfactory first approximation for $\phi(x)$ is obtained by solving, iteratively, the charge-neutral approximation of Poisson's equation, i.e.,

$$n_1^+ + n_2^+ = n_1^- + n_2^- \quad . \tag{1}$$

Once $\phi(x)$ has been determined for all x, the charge separation electric field, E(x), can also be evaluated as $-d\phi/dx$. Finally, the Laplacian of $\phi(x)$ (i.e., $d^2\phi/dx^2$) can be calculated to estimate the value of the electric charge density $e(n^+ - n^-)$ associated with $\phi(x)$. It is shown, a posteriori, that the actual charge separation relative density $(n^+ - n^-)/n^+$ is indeed a small quantity throughout the whole plasma sheath; i.e., that (1) is a valid first approximation and substitute for Poisson's equation.

In the next section we present numerical results corresponding to a solution of equation (1) for which the electric potential ϕ_1 at $x = -\infty$ is equal to ϕ_2 at $x = +\infty$. A wider family of solutions for which $\phi_2 - \phi_1 = 0$ is discussed in Roth et al. (1986).

The partial current densities ($j_{1,2}^{+,-}$) carried by the ions and electrons drifting in the electric field E(x) and magnetic fields B(x) are also analytical expressions of $\phi(x)$ and a(x). The currents produce diamagnetic effects which determine the variation of a(x) and consequently of $B_z(x)$, the z-component of curl a. The vector potential a(x) is solution of Maxwell's euations:

$$B_z = da/dx \text{ and } dB_z/dx = -\mu_o(j_1^+ + j_2^+ - j_1^- + j_2^-) \quad . \tag{2}$$

The standard predictor-corrector Hamin method for numerical integration of equation (2) can be used to obtain the value of a(x) for all x, across the diamagnetic plasma layer (Ralston and Wilf, 1965). Since the magnetic field does not change direction, a(x) is an increasing function of x; it varies from $a = -\infty$ at $x = -\infty$ to $a = +\infty$ at $x = +\infty$.

III. NUMERICAL RESULTS

Figures 1a and 1b show the distributions of $n_{1,2}{}^{+,-}$, the partial ion and electron density distributions as a function of x. The upper horizontal scale represents x in kilometers. The lower scale of the left-hand panels corresponds to x in units of proton gyroradii. The x's in the lower scale of the right-hand panels are expressed in electron gyroradii. Note in the left-hand side panels the smooth variation of the densities over distances of 2-3 ion Larmor gyroradii, i.e., 500-800 km. In the middle of this broad transition region near x = 0, there is a much sharper transition where all densities change significantly over distances of 2-3 electron Larmor gyroradii, i.e., 6-9 km (see enlargement in the right-hand side panels).

Panels c1 and c2 in Figure 1 show the total ion density, $n^+ = n_1{}^+ = n_2{}^+$, which according to the charge neutral equation (1),is equal to the total electron density $n^- = n_1{}^- + n_2{}^-$.

Panels d1 and d2 illustrate how $\theta^{+,-}$, the total ion and electron temperatures vary in the transition region: $\theta^{+,-} = (n_1{}^{+,-}\theta_1{}^{+,-} + n_2{}^{+,-}\theta_2{}^{+,-})/(n_1{}^{+,-} + n_2{}^{+,-})$. Note again the broader scale of variation in the left-hand side panels and the much sharper decrease of θ^- near x =, illustrated in the right-hand side panel.

The distribution of the magnetic field $B_z(x)$ is shown in panels e1 and e2. The magnetic field intensity is equal to 40 nT at $x = -\infty$; this is a typical value of B in the plasmasheet chosen as boundary condition on side 1 at $x = -\infty$. The value of $B_z(x)$ increases to 66.4 nT at $x = +\infty$ with an enhanced variation near x = 0 due to the diamagnetic current contributed by the electrons in the thin electron sheath. It could be shown that the sum of the magnetic pressure and kinetic pressure is precisely a constant throughout the plasma layer.

The electric potential distribution shown in panels f1 and f2 is a continuous function of x. The potential difference between $x = -\infty$ and $x = +\infty$ is equal to zero in the case considered. But similar continuous solutions have been obtained for positive and negative values of $\phi_2 - \phi_1$ of the order of $\pm k T_{1,2}{}^{+,-}/e$ (see Roth et al. 1986). The gradient of the electric potential has a different direction in the electron layer near x = 0 than on both sides in the proton layer. This is also illustrated in the next panels (g1 and g2) showing the electric field intensity which is perpendicular to the surface of the plasma layer: E_x has a large negative value of -220 mV/m in the middle of the thin electron layer. This charge separation electric field accelerates the hotter and more numerous electrons from side 1 toward region 2. On both sides of the electron layer E_x has smaller positive values, not exceeding 2.5 mV/m. This electric field tends to accelerate the hotter and more numerous protons of side 1 toward the cooler and less dense region 2.

The relative electric space charge density deduced from $d^2\phi/dx^2$ is given in panels h1 and h2. It can be seen that $|n^+ - n^-|/n^+$ is smaller than 2 percent within the electron layer; it is smaller than 3×10^{-6} in the ion layer. This confirms a posteriori that charge-neutrality is satisfied to a very good approximation. This confirms also that the solution of equation (1) gives a satisfactory approximation $\phi(x)$ for the electric potential distribution throughout the whole transition.

The average bulk speed of the protons and electrons is given in kilometers per second in the panels i1 and i2: $V^{+,-} = (n_1{}^{+,-}V_1{}^{+,-} + n_2{}^{+,-}V_2{}^{+,-})/(n_1{}^{+,-} + n_2{}^{+,-})$. In the left-hand panel note the large ion jet velocity of more than 500 km/s. V^+ is parallel to the plasma layer and perpendicular to the magnetic field direction. These large ion jets (or ion beams) are spread over a distance of several hundred kilometers. Even more surprising is the narrow jet sheath of electrons with a velocity of the order of 10,000 km/s near x = 0 (see panel i2). These bulk speeds result from the acceleration of charges by the inhomogeneous electric field E(x) and from their deflection in opposite direction by the non-uniform magnetic field B(x).

Panels j1 and j2 give the value of $A = (V^+ - V^-)/U^+$ across the plasma layer; U^+ is the average thermal ion speed. When A is larger than unity, the plasma is unstable. Indeed $A = 1$ corresponds to the threshold for the modified two-stream instability (McBride et al., 1972) also called the lower-hybrid drift instability. It can be seen that in the ionic layer, outside the thin electron layer, $A < 1$; therefore, the parts of the plasma layer on both sides of the electron layer are stable, at least with respect to the modified two-stream instability. However, the thin electron sheath near $x = 0$ is highly unstable and consequently is a potential source for large-amplitude electrostatic waves. These waves can then interact with the electrons, change their pitch angles, and fill the atmospheric loss cone.

As a result of wave-particle interactions, the initially anisotropic (truncated) electron velocity distribution becomes more isotropic until A is equal to or lower than unity: the instability is then quenched. However, as long as the velocity distributions of the electrons have not become isotropic everywhere between $x = -\infty$ and $x = +\infty$, unstable electrons layers will form and generate electrostatic noise.

IV. DISCUSSION AND CONCLUSIONS

The results of the stationary kinetic model illustrated in this paper indicate a number of features pertinent to the study of plasma layers which are associated with discrete auroral arcs.

1. First of all, for the boundary conditions considered (i.e., different densities and temperatures of the electrons and ions on both sides of the plasma layer), the electric potential $\phi(x)$ is not constant, although $\phi(-\infty)$ and $\phi(+\infty)$ are imposed to be equal to zero at $x = \pm\infty$. This indicates that a plasma layer like that studied by Harris (1962) and Alpers (1969), where it is assumed that $\phi(x) = 0$, is by no means a unique nor a general solution.

2. The characteristic scales of variation of the plasma and field variables are the average ion Larmor radius for the broadest structure and the average electron Larmor radius for the thinner embedded electron sheath. If the wider scale of variation is typically 500-800 km in the equatorial plane of the magnetosphere at $L = 10$, its extent projected in the ionosphere is 30 times smaller, i.e., 15-30 km. This corresponds almost to the extent of inverted-V regions near discrete auroral arcs. It corresponds also to the region over which auroral field-aligned potential differences vary significantly.

3. Superimposed on these broad regions of potential variation are often much narrower ones (only a few hundred meters in extent) where sharp potential gradients are observed. We suggest that these thin regions with large electric field intensities are associated with electron layers in the magnetosphere like that found in our kinetic model calculation. The minimum thickness of these electron layers is 5-9 km in the plasmasheet. One can imagine velocity distributions for which there are several electron sheaths embedded in one broader ion structure. The thickness of 5-9 km is a minimum one; indeed electron sheaths are unstable with respect to the modified two-stream instability or lower-hybrid drift instability. Therefore, pitch angle scattering or diffusion of the electrons as a result of wave-particle interactions within these regions eventually tend to make the electron velocity distribution more isotropic. As a consequence the electron sheath tends to broaden and eventually to disappear when the velocity distribution of electrons has become isotropic within the plasma cloud and in the ambient background plasma.

4. Although in our one-dimensional model there is no proper atmospheric loss cone for the plasmasheet electrons, one can easily imagine that for a three-dimensional plasma layer in the magnetosphere the modified two-stream instability can similarly be a source for pitch angle scattering of the electrons and for filling of the atmospheric loss cone. To aliment this source of auroral electron precipitation it is necessary, however, to maintain the electron sheath unstable for the whole lifetime of the discrete auroral arc. Therefore, the plasma layer must constantly be reforming for instance by convection of the plasma cloud "surfing" earthward in the ambient plasmasheet background.

5. The peak value of -200 mV/m for the electric field intensity obtained in our kinetic model calculation is probably excessive. Indeed, the wave-particle diffusion mechanism mentioned above, will smooth irreversibly any too large electric potential gradient. Furthermore, such large perpendicular magnetospheric electric fields (EMF), when mapped down at ionospheric altitudes, must drive very large Pedersen and Hall electric currents through the resistive ionosphere. The Joule dissipation of these currents increases the local plasma temperature. But the local ionization density is then enhanced not only by the increased plasma temperature but also by primary auroral electron bombardment. All these effects concur to enhance the local electric conductivity and to short-circuit the ionospheric load. The large potential gradients applied across the magnetospheric plasma sheath are then discharged as the ionospheric resistance becomes vanishingly small. Magnetospheric potential differences (EMF) perpendicular to magnetic field lines then become field-aligned potential differences accelerating auroral electrons downward along auroral arc magnetic field lines.

6. Ion beams streaming earthward and/or tailward are typical features in the plasmasheet boundary layer adjacent to the tail lobe. These ion beams are observed from high energies of tens of keV to low energies of tens of eV (Lui et al., 1983). Occasionally, these ion beams are found within the plasma sheet proper, near its outer boundary where irregular magnetic field intensities are generally observed. Sugiura et al. (1970) have interpreted these irregular B-field variations as being diamagnetic signatures of spatial plasma clouds for which β is of the order of unity or larger (see also Meng and Mihalov, 1972). Both the ion beam streaming and the change in the magnetic field intensities are inherent in the kinetic model illustrated in Figure 1. It is suggested that ion beam streaming observed at the outer edge of the plasmasheet results from the electric field acceleration and magnetic field deflection of charge particles in plasma layers separating a hot plasma cloud and the cooler ambient plasmasheet or two adjacent diamagnetic plasma clouds of different densities, different temperatures, and different magnetizations, as in our kinetic model.

7. Changing boundary conditions at $x = \pm\infty$ ($N_{1,2}^{+,-}$, $T_{12,,}^{+,-}$) and the choice of the velocity distributions $f_{1,2}^{+,-}$, one can generate a wide variety of different plasma and field distributions within the plasma layer. The plasma layer shown in Figure 1 is only an illustrative example for a magnetospheric EMF source. From this case study one can deduce orders of magnitudes for maximum electric potential gradients (i.e., charge separation electric field), as well as for the maximum velocity of ion beams or jets expected in such plasma layers. By adjusting these boundary conditions and by adequately choosing $f_{1,2}^{+,-}$, it is likely that such kinetic model calculations will be able to simulate a variety of detailed plasma and field measurements across plasma layers or boundaries when available from instruments with high enough time resolution.

The temperature $\theta(x)$ and density $n(x)$ of each plasma species vary across the potential layer separating the hot plasmasheet cloud at $x = -\infty$ from the cooler background magnetotail plasma at $x = +\infty$. The layers considered here [for different values of $\phi_2 - \phi_1 = \phi(+\infty)$] have boundary conditions listed in Table 1. B_{sh} denotes the value of the magnetic field at $x = -\infty$, i.e., deeply inside the plasmasheet cloud. The lower indices sh and t refer to the plasmasheet cloud and background magnetotail particles, respectively, while the upper indices (-) and (+) refer to electrons and protons, respectively. The following notations are assumed: $n_{sh}^{+,-}(-\infty) = N_{sh}^{+,-}$; $\theta_{sh}^{+,-}(-\infty) = T_{sh}^{+,-}$; $n_t^{+,-}(+\infty) = N_t^{+,-}$; $\theta_t^{+,-}(+\infty) = T_t^{+,-}$.

The plasma boundary conditions given in Table 1 correspond to two interpenetrated hydrogen plasmas with different characteristics. Therefore, $n_{sh}^{+,-}(+\infty) = 0$ and $n_t^{+,-}(-\infty) = 0$.

TABLE 1. BOUNDARY CONDITIONS

N_{sh}^- cm^{-3}	T_{sh}^- keV	N_{sh}^+ cm^{-3}	T_{sh}^+ keV	N_t^- cm^{-3}	T_t^- keV	N_t^+ cm^{-3}	T_t^+ keV	B_{sh} nT
0.5	2.5	0.5	12	0.15	0.8	0.15	3	40

REFERENCES

Alpers, W., *Astrophys. Space Sci., 5,* 425-537 (1969).

Botticher, W., H. Wank, and E. Schulz-Gulde (editors), *Proceedings of International Conference on Phenomena in Ionized Gases,* Dusseldorf, August 29-September 2, 1983, pp. 139-147, 1983.

Harris, E. G., *Nuovo Cimento, 23,* 115-121 (1962).

Lemaire, J., and L. F. Burlaga, *Astrophys. Space Sci., 45,* 303-325 (1976).

Lui, A. T. Y., T. E. Eastman, D. J. Williams, and L. A. Frank, Preprint APL/JHU 83-22, 1983.

Lyons, L. R., and D. S. Evans, *J. Geophys. Res., 89,* 2395-2400 (1984).

McBride, J. E., E. Ott, J. P. Boris, and J. H. Orens, *Phys. Fluids, 15,* 2367-2383 (1972).

Meng, C. I., and J.D. Mihalov, *J. Geophys. Res., 77,* 4661-4669 (1972).

Ralston, A., and H. S. Wilf, *Méthodes Mathématiques Pour Calculateurs Arithmétiques,* Dunod, Paris, 482 pp., 1965.

Roth, M., *J. Atmos. Terr. Phys., 38,* 1065-1070 (1976).

Roth, M., *J. Atmos. Terr. Phys., 40,* 323-329 (1978).

Roth, M., in *Proceedings of Magnetospheric Boundary Layers Conference, Alpbach, 11-15 June 1979,* ESA SP-148, edited by B. Battrick and J. Mort, pp. 295-309, ESTEC, Norrdwijk, The Netherlands, 1979.

Roth, M., Ph.D. Thesis, ULB, Brussels, 1980; *Aeronomica Acta A, 221* (1980) (also *Académie Royale de Belgique, Mémoire de la Classe des Sciences,* Collection in 8° - 2e série, T XLIV - Fascicule 7 et dernier, 1984).

Roth, M., D. S. Evans, and J. Lemaire, *J. Geophys. Res.,* submitted, 1986.

Sestero, A., *Phys. Fluids, 7,* 44-51 (1964).

Sestero, A., *Phys. Fluids, 9,* 2006-2013 (1966).

Sugiura, M., T. L. Skillman, B. G. Ledley, and J. P. Heppner, in *Particles and Fields in the Magnetosphere,* edited by B. M. McCormac, pp. 165-170, D. Reidel Publishing Company, Hingham, Massachusetts, 1970.

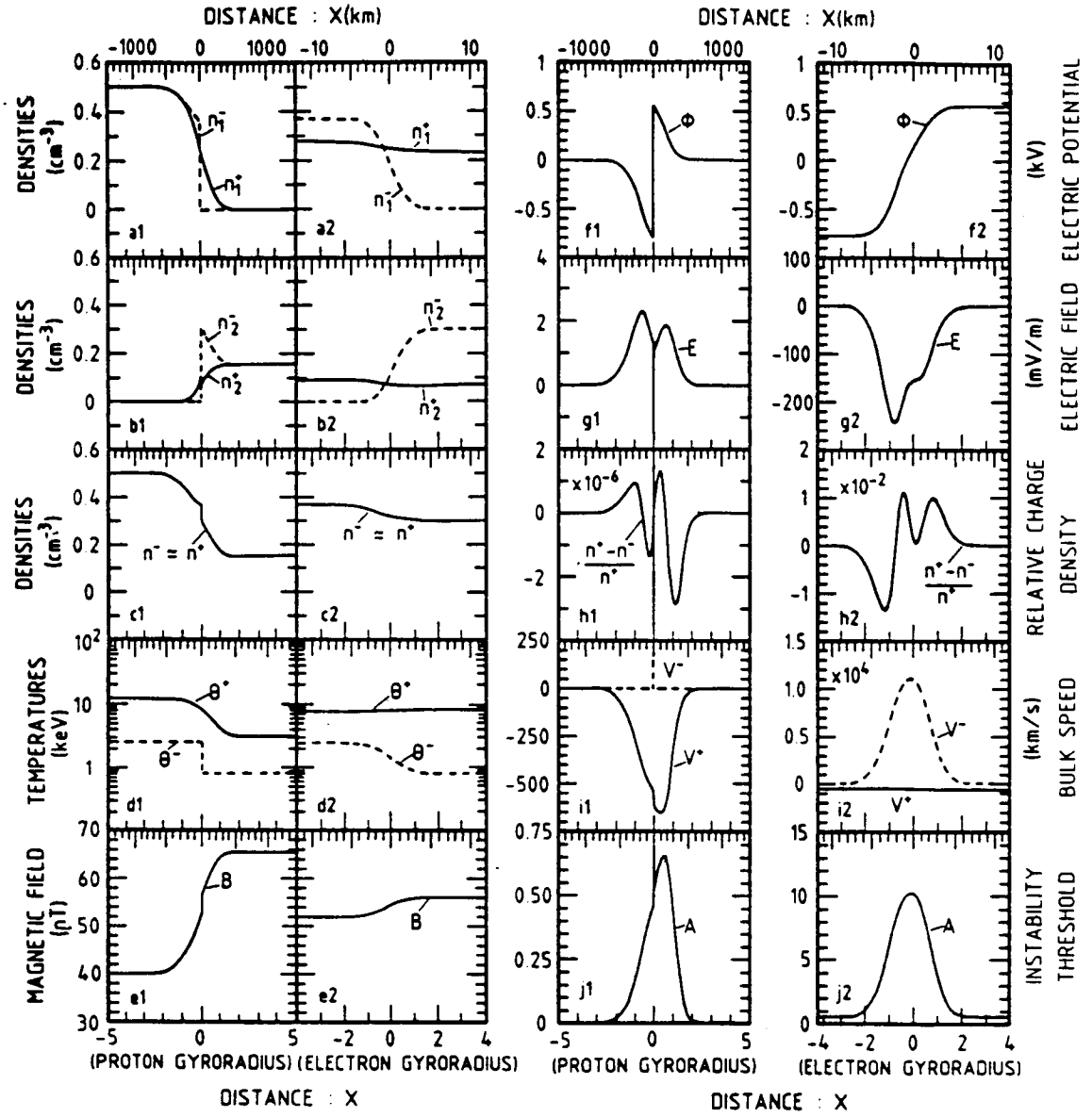

Figure 1. Plasma and field distributions across a plasma layer with boundary conditions typical in the plasmasheet. $\phi(x)$ and $B(x)$ are the electric potential and magnetic field intensity, respectively: ϕ varies from $\phi(-\infty) = 0$ to $\phi(+\infty) = 0$ (see panels f1 and f2); the gradient of ϕ determines the charge separation electric field **E** which is normal to the surface of the plasma layer (see panels g1 and g2); the relative electric space charge density remains small (see panels h1 and h2); the proton (+) and electron (-) densities $n_{1,2}^{+,-}$ from side 1 (i.e., $x = -\infty$) and from side 2 (i.e., $x = +\infty$) vary across the layer from $n_1^{+,-} = 0.5\ cm^{-3}$, $n_2^{+,-} = 0$ at $x = -\infty$ to $n_1^{+,-} = 0$, $n_2^{+,-} = 0{,}15\ cm^{-3}$ at $x = +\infty$ (see panels a1, a2, b1, b2, c1, c2); the proton (+) and electron (-) temperatures $\theta^{+,-}$ vary from $\theta_1^{+} = 12$ keV, $\theta_1^{-} = 2.5$ keV at $x = -\infty$ to $\theta_2^{+} = 3$ keV, $\theta_2^{-} = 0{,}8$ keV at $x = +\infty$ (see panels d1 and d2); the proton (+) and electron (-) bulk velocities $V^{+,-}$ have large peak values in the middle of the composite plasma layer (see panels i1 and i2). Note the very thin electron layer embedded near $x = 0$ within the broader ion layer extending over 4 average ion Larmor gyroradii (see lower scales of left-hand side panels). Expanded views of the narrow electron layer (only 3 or 4 average electron Larmor gyroradii in extent) are shown in the right-hand side panels. The distance x across the planar surface of interface is also shown in kilometers by the upper scales. The thin electron layer is unstable with respect to the modified two-stream instability. Indeed the instability threshold A (see panel j2) exceeds unity in this narrow region where extremely large (and unstable) E-fields are generated.